Article

Cell-Size Homeostasis and the Incremental Rule in a Bacterial Pathogen

Maxime Deforet,[1] Dave van Ditmarsch,[1] and João B. Xavier[1,*]
[1]Program in Computational Biology, Memorial Sloan-Kettering Cancer Center, New York, New York

ABSTRACT How populations of growing cells achieve cell-size homeostasis remains a major question in cell biology. Recent studies in rod-shaped bacteria support the "incremental rule" where each cell adds a constant length before dividing. Although this rule explains narrow cell-size distributions, its mechanism is still unknown. We show that the opportunistic pathogen *Pseudomonas aeruginosa* obeys the incremental rule to achieve cell-length homeostasis during exponential growth but shortens its cells when entering the stationary phase. We identify a mutant, called *frik*, which has increased antibiotic sensitivity, cells that are on average longer, and a fraction of filamentous cells longer than 10 μm. When growth slows due to entry in stationary phase, the distribution of *frik* cell sizes decreases and approaches wild-type length distribution. The rare filamentous cells have abnormally large nucleoids, suggesting that a deficiency in DNA segregation prevents cell division without slowing the exponential elongation rate.

INTRODUCTION

Bacteria exist in a wide diversity of sizes that can span six orders of magnitude, but individual cells within a species maintain regular shape (1–5). How this cell-size homeostasis is achieved remains a topic of intense research (6–13). Recent studies in bacteria propose that rod-shaped bacteria such as *Escherichia coli* and *Bacillus subtilis* follow an incremental rule (also known as the "adder") (6,7,11,12,14), whereby each cell adds a constant volume to their cell body before dividing. New studies take advantage of technical advancements in microfluidics and live-cell imaging to follow thousands of cell divisions. Rod-shaped bacteria have fairly constant cell width, which means that cell length may be used as a proxy for size. The increment in cell length before division is independent of cell's length at birth, ruling out alternative size-regulation rules such as the "timer", according to which cells would divide at regular intervals, and the "sizer", where cells would divide when reaching a maximum size (7,11,12).

In a timer model, any noise in the regulatory mechanism would lead to fluctuations in the time of division (Δt), causing the distribution of cell sizes to spread out over consecutive divisions; but that is not the case here. The sizer model is mostly rejected because the cell-size increment at division (ΔL) does show anticorrelation with cell size at birth (L_b), as predicted by that model. L_b and ΔL are in fact uncorrelated, which supports a constant increment. The incremental rule provides a simple explanation for why variations in cell size converge to the population average without the need for additional regulatory mechanisms (15). The rule works even in the presence of random fluctuations in ΔL (11).

Despite the elegant simplicity of the incremental rule, its mechanism remains unknown. However, it is well known that populations grown in nutrient-poor media grow at a slower exponential growth but still have cell-size homeostasis (12,16). The same happens in mutants defective in sugar uptake (7). Cells that grow more slowly due to nutrient limitation adjust ΔL to a smaller value so that their mean cell size becomes shorter, a relation called the "growth law" (12,16), suggesting that the increment is coupled to the growth rate. This is an important point because exponentially growing cells could, in theory, keep the same size distribution even when growing at a slower growth rate simply by increasing the time between divisions. It also means that experiments that manipulate growth rate by imposing nutrient limitations may not be the best way to discern the mechanism for the incremental rule (11,12). Conversely, a mutation that alters the location of cell division in *E. coli* (Δ*minC*) increases variability of cell lengths without significantly affecting the population average, but individual cells still initiate division only once after a constant increment (7). This experiment shows that the incremental regulation works over a wider range of lengths. Δ*minC* cells have a moderate nucleoid segregation defect leading to a small fraction of cells elongating abnormally. This raises the question of how defects in DNA segregation influence incremental regulation of cell division (7).

We investigate cell-size distribution and its dynamics in the opportunistic pathogen *Pseudomonas aeruginosa*. We find that, like *E. coli* and other rod-shaped bacteria, *P. aeruginosa* follows the incremental rule for cell-size homeostasis. We also investigate an elongated mutant

Submitted April 16, 2015, and accepted for publication July 2, 2015.

*Correspondence: xavierj@mskcc.org

Maxime Deforet and Dave van Ditmarsch contributed equally to this work.

Editor: Dennis Bray.

© 2015 by the Biophysical Society

0006-3495/15/08/0521/8

http://dx.doi.org/10.1016/j.bpj.2015.07.002

isolated from an evolutionary experiment (17), called *frik* due to its aspect ratio resembling a frikandel sausage. *Frik* has a drastically different size distribution than wild-type but also follows the incremental rule with a cell-length increment set to a larger value. A fraction of *frik* cells become hyperelongated, easily surpassing 10 μm in length, which correlates with an abnormal nucleoid. Finally, we find that *frik* cells are more sensitive to clinically relevant antibiotics, a finding that links defects in cell-size regulation to antibiotic susceptibility in this major pathogen.

MATERIALS AND METHODS

Agar pad imaging

All chemicals and reagents were purchased from Fischer Scientific (Pittburgh, PA) unless otherwise noted. Overnight cultures were diluted 100-fold and left to grow for 3.5 h to get the cells to exponential growth. Cells were inoculated onto an agar pad (18), with M9 minimal media (19), either undiluted or diluted 10-fold. Images were taken every 2 min for 7 h using an Axio Observer Z1 inverted microscope, equipped with Definite Focus and a 100×/1.4 oil DIC lens (Carl Zeiss, Thornwood, NY). Cell length at division (L_d) was measured with the image-processing package FIJI (http://fiji.sc/Fiji) (20) and the lineage was tracked with the MTRACKJ plugin (from ImageJ, National Institutes of Health, Bethesda, MD) (21). Length at birth (L_b) of daughter cells was defined as one-half of the length of their mother cell (symmetric division is confirmed by measuring L_b/L_d on a subset of our data; see Fig. S2 *B* in the Supporting Material). In the case of evident asymmetric division, manual measurement of daughter-cell lengths was performed.

Swarming

Swarming assays and competitions were performed as previously described in van Ditmarsch et al. (17) and Xavier et al. (19). The selection coefficient is the initial ratio of *frik* to its direct competitor over the final ratio of *frik* to its direct competitor (selection coefficient < 1 means *frik* wins). The inverse selection coefficient of the competition between *frik* and wild-type was published before in van Ditmarsch et al. (17).

Cell-size determinations

From swarms: the washed overnight culture was diluted 20-fold, to ensure a sufficiently small swarm after 20 h of incubation. The swarming edges were covered by an 18 × 18 mm glass coverslip and snapshots were taken with a 1-ms exposure time using a 40× phase-contrast objective and an Orca2-ER charge-coupled device camera (Hamamatsu Photonics, Middlesex, NJ) mounted on an Axio Observer Z1 inverted microscope (Carl Zeiss). Only the first three cell rows into the swarms were measured manually using FIJI (20). At different phases of growth: akin to the growth curve synchronization protocol (22), an overnight culture of green-fluorescent protein (GFP)-tagged cells (*P. aeruginosa attB*::$P_{A1/04/03}$-*gfp*) was washed and media were inoculated at a final OD_{600} of 0.0025 ODU for the lowest dilution. The first dilution below that was 4096-fold lower, followed by another five dilution steps of twofold each. Growth was measured on a 96-well plate in eight replicates (by OD_{600}) for 14 h for Luria broth (LB) and casamino acid media, 32 h for glycerol media, and 24 h for glucose media. After growing the cells, 2 μL of bacteria were placed on a glass slide and covered with an 18 × 18 mm glass coverslip, followed by exposure to an Hg lamp and imaging with a 63× oil-immersed fluorescent objective (500 ms exposure). Images were processed using custom scripts written in the software MATLAB (The MathWorks, Natick, MA), which calculated an optimal threshold for segmentation. Then morphomathematical operators were used to extract cell length (skeletonization, geodesic distance transformation). Very long cells (outliers) were removed from the *frik* dataset for average cell-length calculation in Fig. 1 *D*. We never observed wild-type (wt) cells longer than 1.5 times the average length; therefore, we chose this cutoff rule for *frik*. For each condition, 100–400 cells were measured. Cell width was measured as the full width at half-maximum of GFP intensity, along a cross section through the cell body.

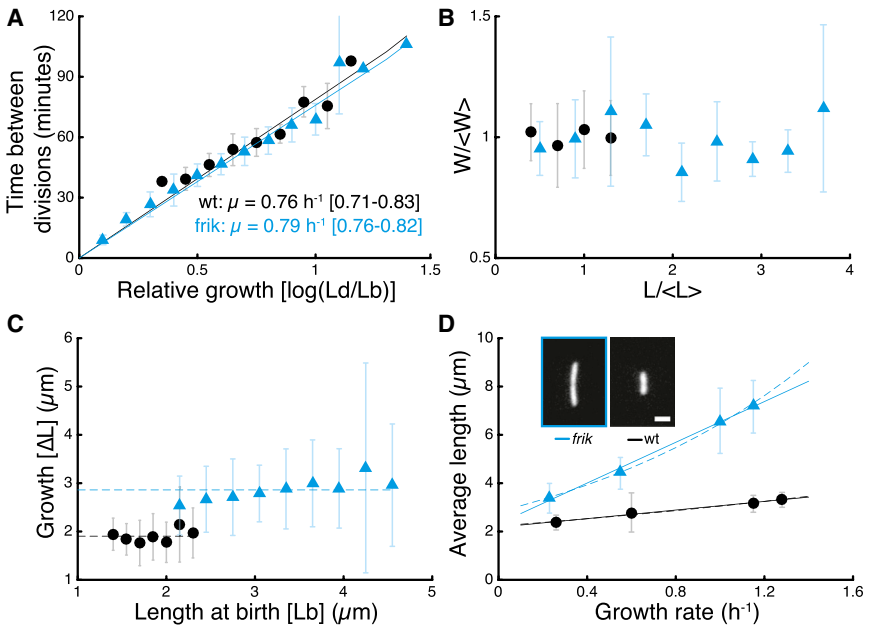

FIGURE 1 Cell-size regulation in *Pseudomonas aeruginosa* and its elongated mutant *frik*. (*A*) Correlation between relative growth ($\log(L_d/L_b)$) and time between divisions reveals identical growth rates in both strains. Binned data. (*B*) Cell width in exponential growth is independent of cell length in both wild-type and *frik* (Pearson correlation coefficient: 0.061 (wt) and −0.039 (*frik*)). Data are rescaled by average length and width for each strain. Average cell length is 3.14 μm for wt and 5.60 μm for *frik*. Average cell width is 0.75 μm for wild-type and 0.74 μm for *frik* ($p = 0.58$, $N = 117$ for wild-type and $N = 107$ for *frik*). (*C*) There is no correlation between growth from birth to division ($\Delta L = L_d$-L_b) and length at birth L_b (Pearson correlation coefficient: −0.010 (wt) and 0.114 (*frik*)). (*D*) Cell lengths measured in exponential growth in different liquid media show that wild-type and *frik* follow the growth law. Media used were (from slowest to fastest) minimal glycerol media, minimal glucose media, casamino acid media, and LB. Error bars are 25 and 75% percentiles. Linear fits (*solid lines*) are $L = 0.89\ \mu + 2.18$ (μm) for wt, $L = 4.21\ \mu + 2.32$ (μm) for *frik*. Exponential fits (*dashed lines*) are $L = 2.22 \exp(0.32\ \mu)$ (μm) for wt, $L = 2.82 \exp(0.83\ \mu)$ (μm) for *frik*. (*Inset*) Micrographs of a *frik* cell (*left*) and a wt cell (*right*) in casamino acid media, imaged by fluorescence microscopy. Scale bar: 2 μm. To see this figure in color, go online.

Simulations

Experimental distributions of ΔL were fitted with a log-normal distribution using the NLINFIT function from the statistics toolbox of MATLAB. Coefficients and 95% confidence intervals were: $\mu = 0.587$ [0.570 0.603] and $\sigma = 0.220$ [0.206 0.233] for wild-type; and $\mu = 0.979$ [0.965 0.993] and $\sigma = 0.264$ [0.253 0.276] for *frik*. We started the simulations with a single 2-μm-long cell, which grew for 23 generations following constant increment model rules: at generation n, 2^{n-1} cells divide symmetrically at a length $L_d = L_b + \Delta L$, where ΔL was drawn from $f(\Delta L)$ for each cell. Length of the initial cell had no influence on the final outcome.

Staining

Overnight cultures were brought to exponential phase as before. Cell membranes were stained using 1 μg/mL of FM 4-64 dye (Life Technologies, Grand Island, NY). Nucleic material was stained using 10 μg/mL of Hoechst 33342. Nucleoids were condensed using 150 μM of chloramphenicol (23). Proton-motive force was nullified by adding 25 μM of CCCP (carbonyl cyanide 3-chlorophenylhydrazone) (24). Imaging was done in nutrient-deficient agar.

Whole-genome sequencing

Whole-genome sequencing was performed using MISEQ sequencing (Illumina, San Diego, CA) and the software MICROSEQ (Applied Biosystems, Las Vegas, NV) with 250 × 2 paired-end reads, yielding an average coverage of 50–70×. Mutations were called using the program BRESEQ (http://barricklab.org/twiki/bin/view/Lab/ToolsBacterialGenomeResequencing) (25) and then verified through Sanger sequencing. Previous sequencing was performed on the SOLiD platform (Applied Biosystems) using 50-bp reads (17).

Minimal inhibitory concentration measurements

Ten twofold dilutions were made for ampicillin (1024 μg/mL and lower), gentamicin (8 μg/mL and lower), tetracycline (16 μg/mL and lower), chloramphenicol (64 μg/mL and lower), and ciprofloxacin (0.5 μg/mL and lower). For all antibiotics, except ampicillin, dilutions were made directly in a transparent 96-well plate (Becton Dickinson, Franklin Lakes, NJ) with a final volume of 150 μL of LB media per well, taking along a control without antibiotics. Both wild-type and *frik* were inoculated directly from glycerol stock into 100 μL of LB-Miller. One microliter of the appropriate cells was then added per well as inoculum. Growth was measured every 10 min through an optical density of 600 nm (OD_{600}) for 24 h. Only for ampicillin, the dilution series was made in 2-mL microcentrifuge tubes, with a final volume of 500 μL for either strain per concentration, again inoculating with 1 μL of the cell suspension. A quantity of 3 × 150 μL per dilution step, and per clone, was transferred to a 96-well plate. Growth was measured as before. Three replicates were used (with three technical replicates each for ampicillin), averaging the final 15 measurement points for each sample. Mean and standard deviations are plotted. IC_{50} values were determined using a four-parameter logistic nonlinear regression. Fitting was carried out in the software MATLAB (The MathWorks) with a custom script using the statistics toolbox FMINSEARCH function:

$$y = \frac{(\text{top} - \text{bottom})}{1 + 10^{(\log(\text{IC}_{50}) - x) \times \text{HillSlope}}} + \text{bottom}.$$

The top and bottom were defined as the highest and lowest measurement, with the approximation for the IC_{50} being in the middle of those two points. The starting Hill coefficient was chosen at 0.8. The FMINSEARCH function then optimized each parameter, using a maximum-likelihood approach. The optimized fits are displayed as continuous lines in the plots in Fig. S5.

RESULTS

P. aeruginosa follows the incremental rule

We investigated the dynamics of *P. aeruginosa* cell size in single cells using agar pads and live-cell imaging (18). To determine whether *P. aeruginosa* follows the incremental model (14), we focused on exponential growth. We measured length at birth (L_b) and length at division (L_d), as well as the generation time elapsed between birth and division (Δt) over several generations. Semilog correlation between relative growth (L_d/L_b) and Δt (Fig. 1 *A*) confirms that elongation of *P. aeruginosa* is exponential at the single-cell level, with a specific growth rate of $\mu = 0.76\ \text{h}^{-1}$. Exponential growth is maintained for multiple hours (>5 cell divisions; Fig. 2 *A*). *P. aeruginosa* maintains constant cell width, regardless of the cell length (Fig. 1 *B*), which allows us to use cell length as a proxy for cell size.

Recent studies use sophisticated microfluidics to maintain a constant influx of nutrients and allow cells to be tracked in time indefinitely (6,7,12). Agar pads have a limited time window of exponential growth but the data acquired suffices to confirm that the incremental model applies to *P. aeruginosa*. First, we observed that ΔL (= L_d-L_b) and L_b are not correlated (Fig. 1 *C*), thereby ruling out the sizer model, where ΔL and L_b would be negatively correlated. Second, a negative correlation between Δt and L_b (Fig. S1 *A*) rules out the timer model, which requires a constant generation time. Several inheritance properties from lineages give further support to the incremental model. For example, there is no correlation between $\Delta L^{\text{daughter}}$ and ΔL^{mother} (Fig. S1 *B*), supporting a random distribution of ΔL ($\langle \Delta L \rangle = 1.82 \pm 0.44\ \mu$m). Moreover, L_b^{mother} and L_b^{daughter} are positively correlated (Fig. S1 *D*), which obeys a rule derived from the incremental model: $L_b^{\text{daughter}} = (L_b^{\text{mother}} + \Delta L)/2$. The slope of 0.5 in this correlation is consistent with cell-size homeostasis. Finally, *P. aeruginosa* cell length is dependent on growth rate, following the so-called growth law (12,16), where cells that grow faster are, on average, longer (Fig. 1 *D*).

Frik mutants: longer cells through larger increment

We then investigated the *frik* mutants—1 of 12 isolated hyperswarmers from an experimental evolution of swarming motility that has a cell-elongation phenotype (17). *Frik* had the highest competitive fitness among all hyperswarmers isolated so far (Fig. S3), but its cell-elongation phenotype is independent of the original mutations identified in hyperswarmers (Fig. S2).

We asked whether *frik* adheres to the incremental rule, despite the cell-elongation phenotype. Indeed, *frik* grows at the same exponential rate as wt in agar pads (Figs. 1 *A* and 2 *B*) with constant width regardless of the length of the cells (Fig. 1 *B*). Furthermore, we saw no correlation

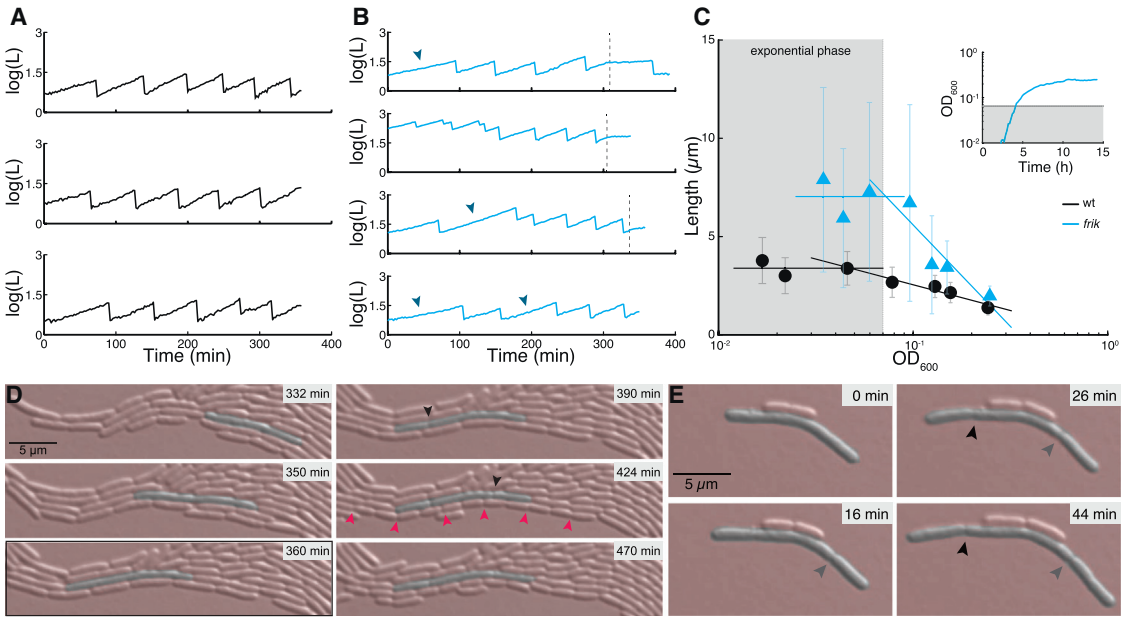

FIGURE 2 Cell growth in agar pads is exponential. (*A* and *B*) Tracking single cells over several hours reveals exponential growth even holds for single cells in both wild-type (*A*) and *frik* (*B*). (*Arrows*) Elongation events that lead to filamentous cells in the *frik* mutant; (*dashed lines*) when growth arrests. (*C*) Both wild-type (*black*) and *frik* (*cyan*) have the longest cells in the exponential phase in liquid cultures with a steady decrease as cells transition into the stationary phase. (Straight lines through the various points are guides to the eyes.) (*Inset*) Representative growth curve from which the cell sizes were determined. (*Gray area*) What we call the "exponential" phase. (Anything outside of the *gray area* is considered the "stationary" phase.) (*D*) *Frik* continues to divide even after growth arrests in agar pads. Growth stops after 360 min in this example (indicated by the *black outline* around the picture). After this time, both a long cell and the shorter cells still divide to become shorter. (*E*) *Frik* tends to show budding off of two cells on opposite poles in short sequence. (*Gray arrowhead*) First septation event, followed by a second septation event (pointed out by the *black arrowhead*). To see this figure in color, go online.

between ΔL and L_b (Fig. 1 *C*), in addition to a negative correlation between Δt and L_b (Fig. S1 *A*). These correlations confirm that *frik* also follows the incremental rule. The increment between divisions for *frik* is larger than for wt (2.82 $\pm$ 1.02 μm for *frik* and 1.82 $\pm$ 0.44 μm for wt). Thus, *frik* overrides the normal increment for *P. aeruginosa* but still keeps a constant ΔL, suggesting that the greater amount of added material is subject to stringent regulation nonetheless.

Frik not only follows the incremental rule, albeit with a different ΔL than wt, it still also obeys the growth law, but again with marked cell-size differences compared to wt (Fig. 1 *D*). It is well known that bacterial cells shorten when entering the stationary phase. By measuring the size distributions of bacteria sampled at distinct times during the growth phase we observed that this is not only the case for wt, but also for *frik* (Fig. 2 *C*). Intriguingly, the average cell size of *frik* decreases much more rapidly than wt, and eventually even reaches a similar mean length as wt.

Rare elongation events explain filamentous *frik* cells

Frik cells are longer than wt on average, but there are occasionally filamentous cells with length longer than 10 μm (Fig. S2). The absurdly long cells account for ~15% of the *frik* population obtained from liquid culture, causing the distribution of L_d to be skewed (*frik* skewness = 2.45; wild-type skewness = 1.19) (data points in Fig. 3 *A*). How do cells >10× the median length arise despite cell-size regulation? To answer this question, we simulated cell divisions following the incremental rule. Drawing only ΔL from experimental distributions, we could recapitulate experimentally observed L_d distributions for *frik* and wild-type fairly well (*lines* in Fig. 3 *A*), except for the tail of the distribution of *frik*. This suggests that a separate process is required to explain the occurrence of filamentous cells. Even though the L_d distributions of wt and *frik* collapse nearly entirely when normalizing by ΔL, the tail is maintained in the distribution of *frik*.

Lineage analysis of *frik* cells reveals that filamentation events are typically restricted to a single lineage (Fig. 3 *B*). Therefore, large fluctuations in ΔL are mostly restricted to the same filamentous cells, rather than following a random pattern within the lineage tree, suggesting that once a cell is filamented, it is more likely to continue disobeying the incremental rule and to continue elongation (Fig. 2 *D*). Interestingly, whenever filamentous *frik* cells do divide they tend to clip at the edges, producing normally sized cells. The clipping can occur from both poles, sometimes one occurring shortly after the other (Fig. 2 *E*), leading to increasingly asymmetrical divisions (Fig. S2 *B*). The smaller cells that arise at either pole behave like normal cells, but the

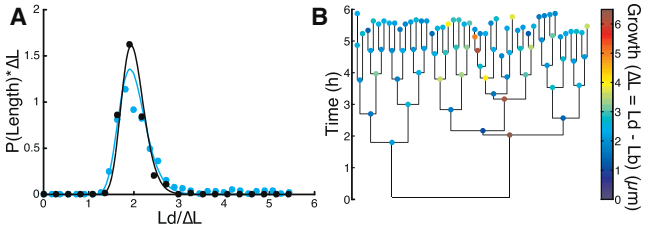

FIGURE 3 The filamentous cell in *frik*. (*A*) Distributions of L_d from experiments (*dots*) and simulations (*lines*). The *X* axis is rescaled with ΔL of each strain. The *Y* axis is rescaled for consistency. (*B*) Lineage tree from one colony of *frik*. To see this figure in color, go online.

remaining long cell keeps elongating before such events happen again.

There are two known types of cell elongation in bacteria: chaining, where the cells stick together after division; and filamentation, where the cell may or may not have septated cellular compartments and is usually multinucleate (26–32). To confirm that the long cells are filamented, we stained the membrane and nucleic material (Fig. 4). Wild-type cells were short and usually not chained together. Whenever this was the case, a typical chain did not consist of more than two cells (presumably two daughter cells from shortly after septation). Each of these cells tended to have one nucleoid. The average short cells in *frik* populations are markedly longer than wild-type cells after the same amount of growth and have a longer nucleoid (Fig. 4 *B* 3). The very long *frik* cells (>10 μm), on the other hand, showed a combination of the two types of elongation (Fig. 4, *B* 1 and 2). There were chains of cells, and very long cells were filamented and multinucleate.

We sequenced the genome of the *frik* mutant with a technology that allows longer reads, and we found two additional mutations in the annotated open reading frames PA14_39100 and PA14_65570. We found that PA14_39100 had a deletion of 12 basepairs in *frik*, but was ruled out as the cause by using microbial genetics. The remaining mutation, a 9-bp deletion in PA14_65570, could thus be the causative mutation. Attempts to recreate this mutant by homologous recombination failed due to difficulties in producing merodiploids, the first step of the protocol. Our failure to manipulate PA14_65570 using molecular techniques suggests that this open reading frame encodes a vital protein, or one whose expression level is highly regulated, so that disruption through allelic replacement may be lethal.

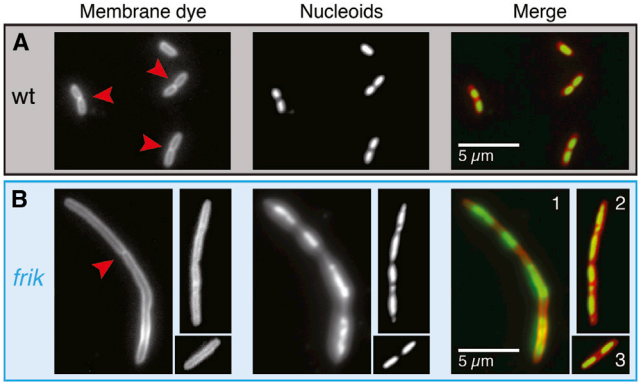

FIGURE 4 *Frik* has longer nucleoids; filamentous cells have abnormal nucleoids. Wild-type (*A*) and *frik* (*B*) from exponentially growing liquid cultures were stained with FM 4-64 (membrane dye) and Hoechst 33342 (a DNA intercalating dye). (*Red arrowheads*) Areas where the membrane has septated. To see this figure in color, go online.

Frik cells have increased sensitivity to antibiotics

Sublethal concentrations of some antibiotics, such as β-lactams, which target penicillin-binding proteins (PBPs), can cause filamentation of bacterial cells, including *P. aeruginosa* (31,33–36). Furthermore, filamentation can be induced in certain bacteria by deleting PBP3 (32). PBPs are responsible for the final steps of peptidoglycan synthesis. *Frik* cells were observed on several occasions to have membrane instabilities (Fig. S4). These combined observations prompted us to evaluate the *frik* antibiotic susceptibility to clinically relevant antibiotics. The antibiotics were chosen to cover most aspects of bacterial biogenesis: cell wall, protein, and DNA synthesis. As expected, *frik* had an increased sensitivity to ampicillin, gentamicin, and chloramphenicol, although not to ciprofloxacin, or tetracycline (Fig. S5).

DISCUSSION

How do single cells regulate their size to achieve homeostatic size distributions even when growing exponentially? The picture that emerges from compiling thousands of cell divisions (7,37,38) is that rod-shaped cells divide after growing a fixed amount of length (ΔL). This manifestation of the so-called incremental rule of cell-size regulation (14) is a passive mechanism that automatically ensures homeostasis by diluting variation over consecutive divisions (7,11,12,38). Nonetheless, the mechanism by which these rod-shaped cells set a constant ΔL remains unknown.

We show for the first time, to our knowledge, that *P. aeruginosa*, an opportunistic pathogen and an important cause of persistent infections (39), obeys the incremental rule. In contrast to recent studies (7,12), our data comes not from microfluidics but from agar pad experiments. Agar pad experiments have a lower throughput but, like others before us (38,40), we see that we can still follow cells growing exponentially over several divisions and find correlations that rule out alternative cell-size homeostasis explanations. We observed that the average cell length shrinks as growth slows down in accordance with the growth law (11,16).

We also investigated cell-length distribution dynamics in a *frik* mutant, which has longer cells without a faster growth rate. This mutant was originally isolated from a hyperswarming evolution experiment (17) and is fitter in

swarming competitions against other hyperswarmer clones with shorter cells, suggesting that cell length could be an evolvable trait in swarming. In *E. coli*, cells can filament because of an SOS response (10), and given the standing wave pattern of Min oscillation (41), the expectation is that filamentous cells then divide at quarter positions. *Frik* filaments also show budding off of cells at either pole in short sequence (Fig. 2 *E*), but our data (Fig. S2 *B*) suggests a continuously increasing asymmetry in the division pattern, instead of the quarter positions that would be expected after the standing wave of Min.

Resequencing the genome of *frik* on a different platform allowed us to find one mutated open reading frame, PA14_65570, which we could not rule out. We cannot conclude, however, that this is the causal mutation because we could not manipulate the locus and other mutations could have escaped our analysis. Still, we found numerous orthologs of PA14_65570 in OrtholugeDB (http://www.pathogenomics.sfu.ca/ortholugedb/) (42), which are putative histidine kinases. Histidine kinases, transmembrane proteins that are often involved in two-component signal transduction systems (43), are also found in many different cellular processes such as cell-cycle progression (44), septation (45), sporulation (46), chemotaxis (47), and mechanosensing (48) and thus PA14_65570 could be involved in cell-size regulation in *P. aeruginosa*.

Our data suggest that cell-length regulation could obey a model first proposed by Fantes et al. (49). Importantly, this model still holds true for any system with similar components, such as other two-component systems. Consider a one-dimensional cell growing exponentially, with growth rate μ:

$$\frac{\partial L}{\partial t} = \mu L. \quad (1)$$

Now suppose that histidine kinases (putatively encoded by PA14_65570, or any other hypothetical open reading frame) are evenly distributed over the cell membrane. Because the cell width is constant, the number of kinases H scales with the cell length:

$$H = \alpha L.$$

We speculate that a protein P regulates cell division by triggering septation when it reaches a threshold P^*. Protein P is activated by this unknown histidine kinase at the membrane. Thus, the activation rate scales with the cell size:

$$\frac{\partial P}{\partial t} = \beta H = \alpha\beta L. \quad (2)$$

Combining Eqs. 1 and 2, we obtain

$$dP = \frac{\alpha\beta}{\mu} dL.$$

Integrating this equation from birth ($L = L_B$, $P = P_B$) to division ($L = L_D$, $P = P^*$), we get

$$P^* - P_B = \frac{\alpha\beta}{\mu}(L_D - L_B) = \frac{\alpha\beta}{\mu}\Delta L.$$

After division, proteins P are degraded or deactivated, then $P_B = 0$,

$$\Delta L = \mu\frac{P^*}{\alpha\beta}.$$

Note that assuming an even sharing of the proteins P between the two daughter cells with no degradation, would lead to a sizer model, with $L_D = \mu P^*/\alpha\beta$. This model leads to the incremental rule of cell-size regulation, as ΔL is not correlated with the length at division L_B. The value ΔL depends only on the septation-triggering threshold P^*, the density of kinases α, the rate of activation of the protein β, and the growth rate μ. It also predicts a linear (not exponential) growth law:

$$\langle L \rangle = \frac{\Delta L}{\log(2)} = \mu\frac{P^*}{\log(2)\alpha\beta}.$$

Our experimental measurements agree with a linear dependence of the average cell size with the growth rate (Fig. 1 *D*). Due to the narrow range of accessible growth rates, linear and exponential models of growth law are difficult to discriminate. Data published in previous publications (12,16,50) suggest an exponential growth law but could arguably support a linear growth law as well. If this hypothetical model is correct, it could also explain why ΔL is larger for *frik* cells. Interestingly, using the InterPro (http://www.ebi.ac.uk/interpro/) (51) and TMHMM Server (http://www.cbs.dtu.dk/services/TMHMM/) (52) tools, we see that the 9-bp deletion in PA14_65570 falls in one of the two predicted transmembrane domains (Fig. S6). If this was indeed the mutation driving the *frik* elongation, the phenotype could be caused by a loss of stability of the putative histidine kinase at the membrane and/or its activity, leading to a lower α and/or β, thus greater ΔL.

The model so far ignores the role of DNA replication on cell-size regulation. DNA replication is likely to be coupled to cell division (e.g., Cooper and Helmstetter (53) and Wang and Levin (54)). Even if PA14_65570 is responsible for the *frik* phenotype, there are mechanisms possible other than the putative histidine kinase. For example, PA14_65570 could regulate peptidoglycan synthesis, which would have an indirect role in cell division, a mechanism consistent with the antibiotic sensitivity of *frik* cells. Alternatively, the fragmented localization of DNA revealed by the staining of the *frik* mutant suggests that there may be some DNA damage, and in turn DNA damage could stimulate the SOS response to inhibit cell division. Future studies that unveil the role of DNA replication, chromosome segregation, or DNA replication, for example, because of the presence of multiple

replication forks (50), should shed important light on cell-size regulation and the growth law. It is important to note that our model is not the only model that could explain an increase in ΔL and is purely phenomenological in its setup. Other explanatory models include those that specifically take DNA replication into account, such as the initiator model first stipulated by Cooper and Helmstetter (53), as well as other models describing the C+D phases of bacterial growth (C = chromosome replication, D = time between completion of replication and division) (55).

Our finding that abnormal cell-size regulation increases antibiotic sensitivity has potential therapeutic implications. In a time when antibiotic resistance increases at the global scale and the commercial incentive to develop novel antibiotic is low (56), unveiling mechanisms that sensitize pathogenic bacteria to existing antibiotics by interfering with cell-size regulation is a relevant option (15). Drugs that affect cell size could be used in combination with traditional antibiotics to restore sensitivity in resistant pathogens.

SUPPORTING MATERIAL

Six figures are available at http://www.biophysj.org/biophysj/supplemental/S0006-3495(15)00671-2.

AUTHOR CONTRIBUTIONS

D.v.D. discovered the *frik* phenotype; M.D. developed the model and quantitative analyses; M.D., D.v.D., and J.B.X. designed research; M.D. and D.v.D. performed research; M.D. and D.v.D. analyzed data; and M.D., D.v.D., and J.B.X. wrote the article.

REFERENCES

1. Cabeen, M. T., and C. Jacobs-Wagner. 2005. Bacterial cell shape. *Nat. Rev. Microbiol.* 3:601–610.
2. Dworkin, J. 2010. Form equals function? Bacterial shape and its consequences for pathogenesis. *Mol. Microbiol.* 78:792–795.
3. Männik, J., R. Driessen, …, C. Dekker. 2009. Bacterial growth and motility in sub-micron constrictions. *Proc. Natl. Acad. Sci. USA.* 106:14861–14866.
4. Young, K. D. 2006. The selective value of bacterial shape. *Microbiol. Mol. Biol. Rev.* 70:660–703.
5. Young, K. D. 2007. Bacterial morphology: why have different shapes? *Curr. Opin. Microbiol.* 10:596–600.
6. Amir, A. 2014. Cell size regulation in bacteria. *Phys. Rev. Lett.* 112
7. Campos, M., I. V. Surovtsev, …, C. Jacobs-Wagner. 2014. A constant size extension drives bacterial cell size homeostasis. *Cell.* 159:1433–1446.
8. Di Talia, S., J. M. Skotheim, …, F. R. Cross. 2007. The effects of molecular noise and size control on variability in the budding yeast cell cycle. *Nature.* 448:947–951.
9. Fantes, P. A. 1977. Control of cell size and cycle time in *Schizosaccharomyces pombe*. *J. Cell Sci.* 24:51–67.
10. Iyer-Biswas, S., C. S. Wright, …, N. F. Scherer. 2014. Scaling laws governing stochastic growth and division of single bacterial cells. *Proc. Natl. Acad. Sci. USA.* 111:15912–15917.
11. Jun, S., and S. Taheri-Araghi. 2015. Cell-size maintenance: universal strategy revealed. *Trends Microbiol.* 23:4–6.
12. Taheri-Araghi, S., S. Bradde, …, S. Jun. 2014. Cell-size control and homeostasis in bacteria. *Curr. Biol.* 25:385–391.
13. Wang, P., L. Robert, …, S. Jun. 2010. Robust growth of *Escherichia coli*. *Curr. Biol.* 20:1099–1103.
14. Voorn, W. J., L. J. H. Koppes, and N. B. Grover. 1993. Mathematics of cell division in *Escherichia coli*: comparison between sloppy-size and incremental-size kinetics. *Curr. Top. Mol. Gen.* 1:187–194.
15. Goodsmith, N., X. V. Guo, …, S. Ehrt. 2015. Disruption of an *M. tuberculosis* membrane protein causes a magnesium-dependent cell division defect and failure to persist in mice. *PLoS Pathog.* 11:e1004645.
16. Schaechter, M., O. Maaloe, and N. O. Kjeldgaard. 1958. Dependency on medium and temperature of cell size and chemical composition during balanced growth of *Salmonella typhimurium*. *J. Gen. Microbiol.* 19:592–606.
17. van Ditmarsch, D., K. E. Boyle, …, J. B. Xavier. 2013. Convergent evolution of hyperswarming leads to impaired biofilm formation in pathogenic bacteria. *Cell Rep.* 4:697–708.
18. de Jong, I. G., K. Beilharz, …, J.-W. Veening. 2011. Live cell imaging of *Bacillus subtilis* and *Streptococcus pneumoniae* using automated time-lapse microscopy. *J. Vis. Exp.* 28:e3145.
19. Xavier, J. B., W. Kim, and K. R. Foster. 2011. A molecular mechanism that stabilizes cooperative secretions in *Pseudomonas aeruginosa*. *Mol. Microbiol.* 79:166–179.
20. Schindelin, J., I. Arganda-Carreras, …, A. Cardona. 2012. FIJI: an open-source platform for biological-image analysis. *Nat. Methods.* 9:676–682.
21. Meijering, E., O. Dzyubachyk, and I. Smal. 2012. Methods for cell and particle tracking. *Methods Enzymol.* 504:183–200.
22. van Ditmarsch, D., and J. B. Xavier. 2011. High-resolution time series of *Pseudomonas aeruginosa* gene expression and rhamnolipid secretion through growth curve synchronization. *BMC Microbiol.* 11:140.
23. van Helvoort, J. M., J. Kool, and C. L. Woldringh. 1996. Chloramphenicol causes fusion of separated nucleoids in *Escherichia coli* K-12 cells and filaments. *J. Bacteriol.* 178:4289–4293.
24. Cho, H., Y. Oh, …, Y. Lee. 2001. Concentration of CCCP should be optimized to detect the efflux system in quinolone-susceptible *Escherichia coli*. *J. Microbiol.* 39:62–66.
25. Deatherage, D. E., and J. E. Barrick. 2014. Identification of mutations in laboratory-evolved microbes from next-generation sequencing data using BRESEQ. *Methods Mol. Biol.* 1151:165–188.
26. Vejborg, R. M., and P. Klemm. 2009. Cellular chain formation in *Escherichia coli* biofilms. *Microbiology.* 155:1407–1417.
27. Justice, S. S., D. A. Hunstad, …, S. J. Hultgren. 2008. Morphological plasticity as a bacterial survival strategy. *Nat. Rev. Microbiol.* 6:162–168.
28. Steinberger, R. E., A. R. Allen, …, P. A. Holden. 2002. Elongation correlates with nutrient deprivation in *Pseudomonas aeruginosa* unsaturates biofilms. *Microb. Ecol.* 43:416–423.
29. Werner, E., F. Roe, …, P. S. Stewart. 2004. Stratified growth in *Pseudomonas aeruginosa* biofilms. *Appl. Environ. Microbiol.* 70:6188–6196.
30. Yoon, M. Y., K. M. Lee, …, S. S. Yoon. 2011. Contribution of cell elongation to the biofilm formation of *Pseudomonas aeruginosa* during anaerobic respiration. *PLoS One.* 6:e16105.
31. Rolinson, G. N. 1980. Effect of β-lactam antibiotics on bacterial cell growth rate. *J. Gen. Microbiol.* 120:317–323.
32. Popham, D. L., and K. D. Young. 2003. Role of penicillin-binding proteins in bacterial cell morphogenesis. *Curr. Opin. Microbiol.* 6:594–599.
33. Ellis, L. F., D. K. Herron, …, R. A. Schlegel. 1976. Evaluation of antibiotic efficacy using electron microscopy: morphological effects of guanylureido cephalosporin, chlorobenzoylureido cephalosporin,

BL-P1654, and carbenicillin on *Pseudomonas aeruginosa*. *Antimicrob. Agents Chemother.* 9:334–342.

34. Tomasz, A. 1986. Penicillin-binding proteins and the antibacterial effectiveness of β-lactam antibiotics. *Rev. Infect. Dis.* 8 (*Suppl 3*): S260–S278.
35. Gould, I. M., and F. M. MacKenzie. 1997. The response of *Enterobacteriaceae* to β-lactam antibiotics—'round forms, filaments and the root of all evil'. *J. Antimicrob. Chemother.* 40:495–499.
36. Hanberger, H., L. E. Nilsson, …, R. Maller. 1991. Post-antibiotic effect of β-lactam antibiotics on Gram-negative bacteria in relation to morphology, initial killing and MIC. *Eur. J. Clin. Microbiol. Infect. Dis.* 10:927–934.
37. Yamanaka, K., W. Zheng, …, M. Inouye. 2001. CspD, a novel DNA replication inhibitor induced during the stationary phase in *Escherichia coli*. *Mol. Microbiol.* 39:1572–1584.
38. Soifer, I., L. Robert, …, A. Amir. 2014. Single-cell analysis of growth in budding yeast and bacteria reveals a common size regulation strategy. arXiv.org > q-bio > arXiv:1410.4771.
39. Costerton, J. W., P. S. Stewart, and E. P. Greenberg. 1999. Bacterial biofilms: a common cause of persistent infections. *Science.* 284:1318–1322.
40. Stewart, E. J., R. Madden, …, F. Taddei. 2005. Aging and death in an organism that reproduces by morphologically symmetric division. *PLoS Biol.* 3:e45.
41. Bonny, M., E. Fischer-Friedrich, …, K. Kruse. 2013. Membrane binding of MinE allows for a comprehensive description of Min-protein pattern formation. *PLOS Comput. Biol.* 9:e1003347.
42. Whiteside, M. D., G. L. Winsor, …, F. S. Brinkman. 2013. OrthologeDB: a bacterial and archaeal orthology resource for improved comparative genomic analysis. *Nucleic Acids Res.* 41:D366–D376.
43. Mascher, T., J. D. Helmann, and G. Unden. 2006. Stimulus perception in bacterial signal-transducing histidine kinases. *Microbiol. Mol. Biol. Rev.* 70:910–938.
44. Iniesta, A. A., N. J. Hillson, and L. Shapiro. 2010. Cell pole-specific activation of a critical bacterial cell cycle kinase. *Proc. Natl. Acad. Sci. USA.* 107:7012–7017.
45. Fukushima, T., H. Szurmant, …, J. A. Hoch. 2008. A sensor histidine kinase co-ordinates cell wall architecture with cell division in *Bacillus subtilis*. *Mol. Microbiol.* 69:621–632.
46. Eswaramoorthy, P., D. Duan, …, M. Fujita. 2010. The threshold level of the sensor histidine kinase KinA governs entry into sporulation in *Bacillus subtilis*. *J. Bacteriol.* 192:3870–3882.
47. Güvener, Z. T., D. F. Tifrea, and C. S. Harwood. 2006. Two different *Pseudomonas aeruginosa* chemosensory signal transduction complexes localize to cell poles and form and remould in stationary phase. *Mol. Microbiol.* 61:106–118.
48. O'Connor, J. R., N. J. Kuwada, …, C. S. Harwood. 2012. Surface sensing and lateral subcellular localization of WspA, the receptor in a chemosensory-like system leading to c-di-GMP production. *Mol. Microbiol.* 86:720–729.
49. Fantes, P. A., W. D. Grant, …, A. E. Wheals. 1975. The regulation of cell size and the control of mitosis. *J. Theor. Biol.* 50:213–244.
50. Sharpe, M. E., P. M. Hauser, …, J. Errington. 1998. *Bacillus subtilis* cell cycle as studied by fluorescence microscopy: constancy of cell length at initiation of DNA replication and evidence for active nucleoid partitioning. *J. Bacteriol.* 180:547–555.
51. Mitchell, A., H. Y. Chang, …, R. D. Finn. 2015. The InterPro protein families database: the classification resource after 15 years. *Nucleic Acids Res.* 43:D213–D221.
52. Krogh, A., B. Larsson, …, E. L. Sonnhammer. 2001. Predicting transmembrane protein topology with a hidden Markov model: application to complete genomes. *J. Mol. Biol.* 305:567–580.
53. Cooper, S., and C. E. Helmstetter. 1968. Chromosome replication and the division cycle of *Escherichia coli* B/r. *J. Mol. Biol.* 31:519–540.
54. Wang, J. D., and P. A. Levin. 2009. Metabolism, cell growth and the bacterial cell cycle. *Nat. Rev. Microbiol.* 7:822–827.
55. Hill, N. S., R. Kadoya, …, P. A. Levin. 2012. Cell size and the initiation of DNA replication in bacteria. *PLoS Genet.* 8:e1002549.
56. Nathan, C., and O. Cars. 2014. Antibiotic resistance—problems, progress, and prospects. *N. Engl. J. Med.* 371:1761–1763.

Biophysical Journal

Supporting Material

Cell-Size Homeostasis and the Incremental Rule in a Bacterial Pathogen

Maxime Deforet,[1] Dave van Ditmarsch,[1] and João B. Xavier[1,*]

[1]Program in Computational Biology, Memorial Sloan-Kettering Cancer Center, New York, New York

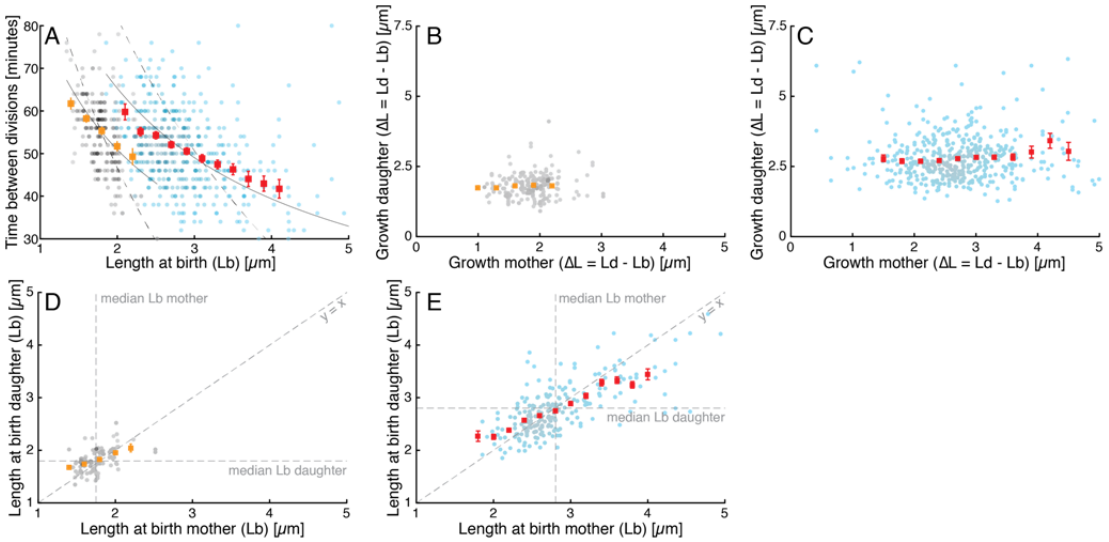

Figure S1: *P. aeruginosa* and the *frik* mutant obey the incremental rule of cell size regulation. For all plots, wt is plotted in black and orange, whereas *frik* is plotted in cyan and red. (A) There is a negative correlation between Lb and ΔT. Solid lines indicate best fits to the incremental model and dash lines indicate best fit to the "sizer" model. (C-D) There is no correlation between Δ^{mother} and $\Delta^{daughter}$. (E-F) $L_b{}^{mother}$ and $L_b{}^{daughter}$ are correlated with a slope of 0.5.

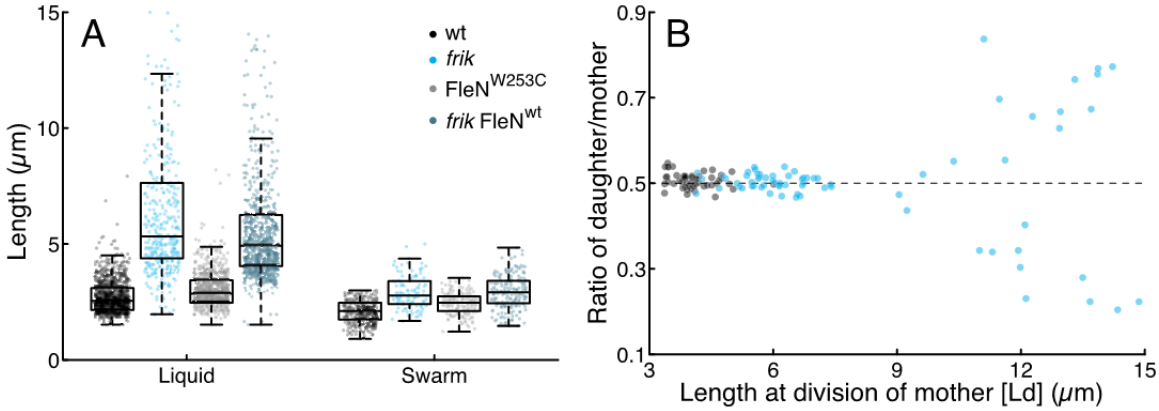

Figure S2: Cell size in *Pseudomonas aeruginosa* and its elongated mutant *frik*. (A) Cell length distributions from exponentially growing liquid cultures and swarms. In liquid culture, *frik* and *frik* $FleN^{wt}$ are longer than wt and $FleN^{W253C}$ (N = 423-897, p <<0.001 by Kruskal-Wallis). *Frik* and *frik* $FleN^{wt}$ are longer than the other two strains when quantifying at swarming edges, as determined by Kruskal-Wallis test (p<<0.001, n = 107-376). (B) Cell division is very symmetric for both wild type (black) and frik cells (cyan), with the exception of the filamentous cell (>10 μm).

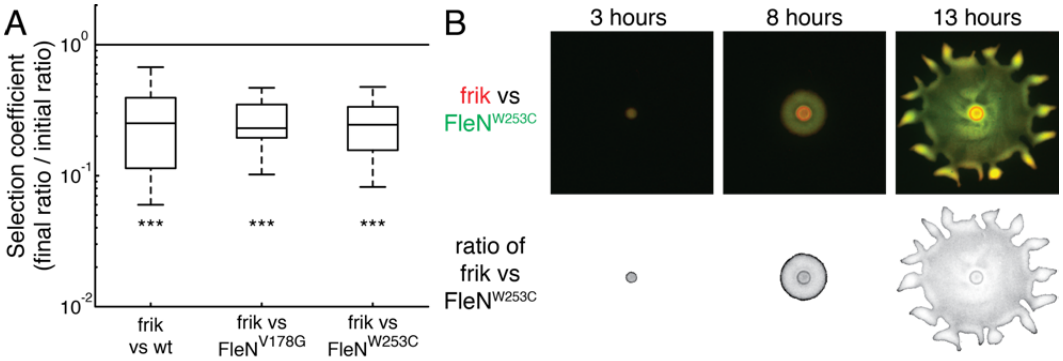

Figure S3: *frik* has a swarming advantage over wild type and other hyperswarmers. (A) Selection coefficients (defined as final ratio over initial ratio) of various clones against *frik*. The horizontal line represents the neutral selection coefficient of 1; anything below that means that the respective clone loses against frik. The (inverse) selection coefficient of *frik* versus wt was previously published [21]. (B) *Frik* segregates at the edge of a swarm from early on. The top row represents fluorescence images and the bottom row is the calculated ratio of *frik* versus FleN^{W253C} based on the fluorescence channels.

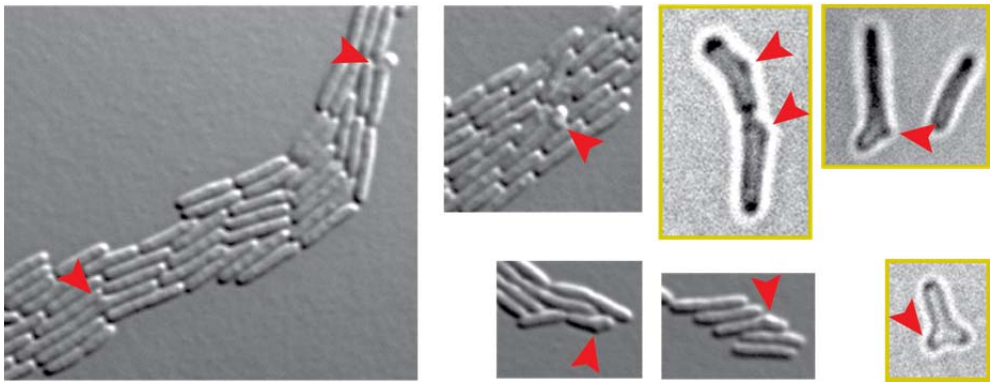

Figure S4: *frik* occasionally shows membrane instabilities. Microscopy pictures taken from either agar pad or liquid culture cells (the latter are outlined in dark yellow) for *frik* shows various cells with membrane instabilities (indicated with red arrowheads).

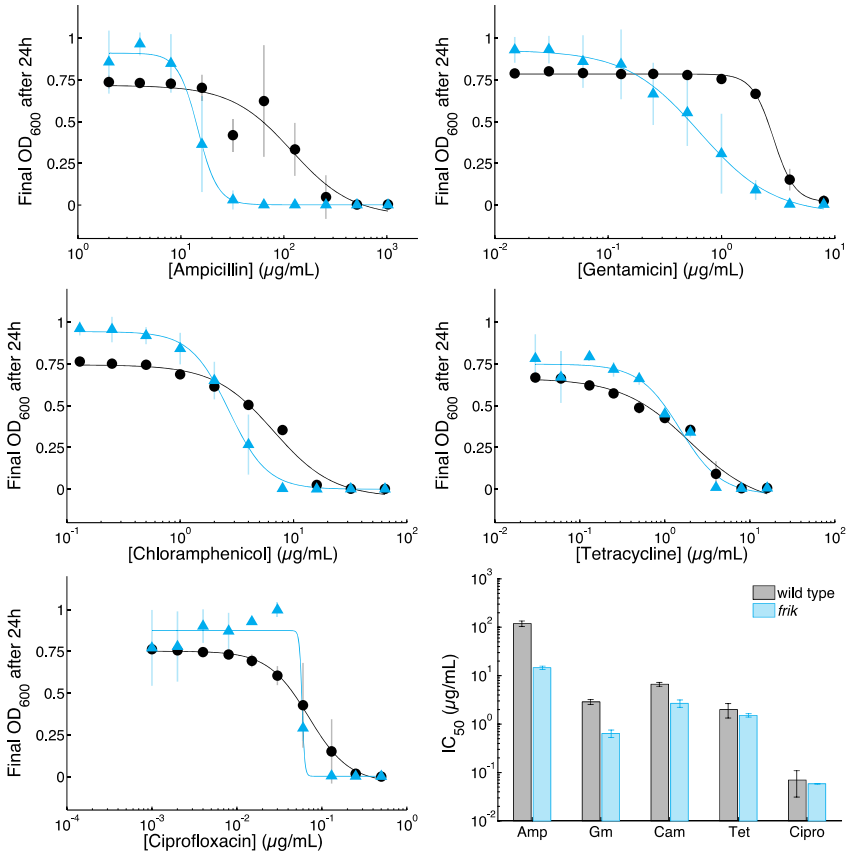

Figure S5: *frik* is sensitive to ampicillin, gentamicin, and chloramphenicol, but not tetracycline, or ciprofloxacin. Minimal inhibitory concentration (MIC) measurements for (A) ampicillin, (B) gentamicin, (C) chloramphenicol, (D) tetracycline, and (E) ciprofloxacin. Black circles represent wild type, cyan triangles represent frik. Mean and standard deviation are plotted. The lines indicate the model fit with which the IC_{50} was determined. (F) The determined IC_{50} values for the various antibiotics with 95%-CI.

wt PA14_65570 amino acid sequence

MTRPTSVKPDNFFLLLFRALRQRRVPIALRLASHSLILVALALLIYAWVMGMQFRQAMQQQADALGQSLITQTAASATELLVSNDILSLNVLLNNLVKNPLVAHAAIYSIDQRILAEAGSRPK(
ATEGLYSTPITFQEVIAGHLRISLDMQQFQQPMMISLQSMGLISLILLILALYFSLRLGRQISTPLLQLRVWLRDPDNPAPGAELQNELGDLARDLEERLVPEKPPAPEPEEAPLPQNFDDILI
ADLRSRKVEASAFEEDDIPLGDALLDETKPVEFTSIDEDPLDQDAFDENGAEAGDQPAAPAAAREPQHSAVLAIQLGAQEQLRRLPRSRLVDLLQRYRDCLEQAARQYKGSLHTLSDGGSLILI
NRADYLTNALCCGELMRALGHALQIEVADSGITLQLQLGLSLGEDLSEQTQADLLLNETVQNALALNQHSRNLLLVERSIADDAVVRERARIRAIASPEGACCVERLLEPYPSMLERQLARMHI

Figure S6: *frik* mutants have a mutation in a putative transmembrane domain in gene PA14_65570. The amino acid sequence encoded by gene PA14_65570 has two predicted transmembrane domains (in red). The 9 base pair deletion found in the *frik* mutant would cause the loss of 3 amino acid residues in one of the transmembrane domains (shown in a rectangle).